[28] Wong, K. T.
Acoustic vector-sensor "blind" beamforming & geolocation for FFH-sources.
IEEE Transactions on Aerospace and Electronic Systems, **46**, 1 (Jan. 2010), 444–449.

[29] He, J., et al.
Particle-velocity-field difference smoothing for coherent source localization in spatially nonuniform noise.
IEEE Journal of Oceanic Engineering, **35**, 1 (Jan. 2010), 113–119.

[30] Wu, Y. I., Wong, K. T., and Lau, S-K.
The acoustic vector-sensor's near-field array-manifold.
IEEE Transactions on Signal Processing, **58**, 7 (July 2010), 3946–3951.

[31] Li, T., Tabrikian, J., and Nehorai, A.
A Barankin-type bound on direction estimation using acoustic sensor arrays.
IEEE Transactions on Signal Processing, **59**, 1 (Jan. 2011), 431–435.

Stochastic Model Based Radar Waveform Design for Weapon Detection

We consider signature exploitation based waveform design for detection of weapons with a single-antenna monostatic radar. In order to account for the target signature variation with orientation and aspect angle, we model the target impulse response as a random process. For a weapon target, we show that the stochastic model based waveform significantly outperforms the commonly used chirp waveform in terms of the signal-to-clutter-and-noise ratio (SCNR) at the output of the receive filter, leading to an enhanced detection performance.

I. INTRODUCTION

Detection of weapons is an area of significant interest to both law enforcement agencies and the military. It is being sought out in a variety of applications, including controlling checkpoints in airports and border crossings, securing public spaces, and enhancing situational awareness inside urban structures by determining the intent of building use [1–8]. Radar technology is the modality of choice since RF signals have the ability to penetrate optically opaque media, such as clothing and construction materials.

Weapon detection RF systems that provide a high-resolution imaging based solution have been reported recently in the literature [1, 6–8]. In [1], [6], a wideband microwave holographic imaging system is described that utilizes phase and amplitude information recorded over a two-dimensional aperture to reconstruct a focused image of the concealed weapons. Near optical quality imaging results are provided using a prototype real-time system operating over the 27–33 GHz frequency band. However, since this system employs millimeter waves, which suffer from very high attenuation on propagation through common construction materials, it is not suitable for detection of weapons inside buildings. A microwave imaging system to detect a cache of weapons concealed in a wall or a floor is proposed in [7]. Examples of detection of targets embedded in

Manuscript received October 8, 2010; revised February 25, 2011; released for publication July 6, 2011.

IEEE Log No. T-AES/48/2/943860.

Refereeing of this contribution was handled by R. Narayanan.

This work was supported in part by the U.S. Army Research Lab under Contract W911NF-07-D-0001.

walls in [7] include electromagnetic (EM) modeling data at frequencies of a few hundred MHz. Such a system may also be used for detection of weapons inside buildings. However, at such low frequencies, the imaging resolution is degraded, rendering it difficult to detect and characterize weapons directly in the image domain. In [8], an approach based on polarimetric radar techniques is proposed for through-the-wall detection of weapons. EM simulation examples in the context of through-the-wall radar imaging are provided that successfully discriminate humans carrying weapons from unarmed humans.

In this correspondence, we propose a data-domain approach to address the problem of weapon detection. More specifically, we design appropriate transmit waveforms and receivers for improved detection of weapons. We focus on simple low-cost single-antenna monostatic radar operation.[1] Since sufficient information about the properties and characteristics of the targets of interest, such as shape, size, and composition, is available a priori through EM modeling and experimentations, we consider waveform design techniques that are based on target signature exploitation, and which make use of the a priori information to achieve higher probability of target detection [9–12]. The optimal approach to this problem is based on the matched illumination signature exploitation concept in which the transmit waveform and the receive filter are designed such that the signal-to-clutter-and-noise-ratio (SCNR) at the output of the receive filter is maximized [9, 10]. This approach, however, assumes perfect knowledge of the target impulse response (range profile), which, in turn, requires knowledge of the target orientation and aspect angle. In practice, this information may not always be available, especially when the target is behind walls or inside enclosed structures. Thus, it is more practical to assume that the target impulse response is a random process, and the impulse responses corresponding to various target orientations and aspect angles are sample functions of this process. A transmit waveform-receive filter combination can then be designed to achieve the best detection performance for the stochastic target in terms of the highest SCNR.

Signature exploitation based radar waveform design problems have been studied for a stochastic target model in [13]–[14] from the SCNR maximization perspective. In [13], a frequency-domain approach is presented which designs the transmit waveform-receive filter combination that maximizes an SCNR bound rather than the SCNR directly. On the other hand, a time-domain approach is considered in [14], wherein an iterative algorithm that guarantees SCNR performance improvement in each iteration step is proposed for multiple-input multiple-output (MIMO) operation to optimize the transmit waveforms and the receive filters. In this correspondence, we employ the time-domain scheme of [14] to design radar waveforms for improved weapon detection for both free-space and through-the-wall scenarios. We consider radars of single antennas, which are most attractive and desirable in many operations. We use an AK-47 assault rifle as the target of interest and design the stochastic model based waveform using the electromagnetically modeled rifle impulse responses. Detection performance of the designed waveform is evaluated in the presence of noise and clutter, and is compared with that of the commonly used chirp signal of the same duration and energy.

The correspondence is organized as follows. Section II summarizes the signal model and the stochastic target based waveform design approach. Section III describes the EM of the AK-47 rifle. Supporting waveform design examples for the AK-47 rifle are provided in Section IV for clutter-free and clutter-plus-noise cases, along with performance comparison with a chirp waveform. Section V contains concluding remarks.

II. SIGNAL MODEL AND WAVEFORM DESIGN

For the extended targets of interest, we consider the linear time-invariant system model over the observation period, as described in [10], [11], [14], [15], which is briefly recalled in this section to make the correspondence self-contained.

Let the finite-energy finite-duration transmitted signal be defined as an $N_z \times 1$ vector $\mathbf{z} = [z_0, z_1, \ldots, z_{(N_z-1)}]^T$, and the target impulse response apparent to the radar be given by an $N_q \times 1$ vector $\mathbf{q} = [q_0, q_1, \ldots, q_{(N_q-1)}]^T$. Then, the noise- and clutter-free received target return is represented by $\mathbf{s} = [s_0, s_1, \ldots, s_{(N_s-1)}]^T$, where $N_s = N_z + N_q - 1$, and can be expressed as

$$\mathbf{s} = \mathbf{Q}\mathbf{z}. \tag{1}$$

Here, $\mathbf{Q}$ is the $N_s \times N_z$ target convolution matrix, given by

$$\mathbf{Q} = \begin{bmatrix} q_0 & 0 & \cdots & 0 \\ q_1 & q_0 & \ddots & \vdots \\ \vdots & q_1 & \ddots & 0 \\ q_{(N_q-1)} & \vdots & \ddots & q_0 \\ 0 & q_{(N_q-1)} & \ddots & q_1 \\ \vdots & \ddots & \ddots & \vdots \\ 0 & \cdots & \cdots & q_{(N_q-1)} \end{bmatrix}. \tag{2}$$

[1] It is noted that the radar could be quasi-monostatic; that is, the transmitting and receiving antennas are separate, but in approximately the same location. The ensuing analysis will be applicable to such quasi-monostatic systems by assuming that the pair of antennas simulate a single antenna, with significantly higher transmit to receive isolation, located at the midpoint between the two antennas.

Likewise, by representing the noise by $\mathbf{v} = [v_0, v_1, \ldots, v_{(N_s-1)}]^T$ and the clutter impulse response matrix as

$$\mathbf{C} = \begin{bmatrix} c_0 & c_{-1} & \cdots & c_{-(N_z-1)} \\ c_1 & c_0 & \ddots & \vdots \\ \vdots & c_1 & \ddots & \vdots \\ \vdots & \ddots & \ddots & c_0 \\ \vdots & \ddots & \ddots & c_1 \\ \vdots & \ddots & \ddots & \vdots \\ c_{(N_s-1)} & 0 & \cdots & c_{(N_q-1)} \end{bmatrix} \tag{3}$$

the received signal can be expressed as

$$\begin{aligned} \mathbf{r} &= \mathbf{s} + \mathbf{C}\mathbf{z} + \mathbf{v} \\ \mathbf{r} &= [r_0, r_1, \ldots, r_{(N_s-1)}]^T. \end{aligned} \tag{4}$$

Accordingly, the system output, after the receiver filter, is given by

$$y = \mathbf{b}^T\mathbf{r} = \mathbf{b}^T\mathbf{s} + \mathbf{b}^T\mathbf{C}\mathbf{z} + \mathbf{b}^T\mathbf{v} \tag{5}$$

where $\mathbf{b} = [b_0, b_1, \ldots, b_{(N_s-1)}]^T$ is the receiver filter impulse response.

Both clutter and noise are assumed to be independent wide sense stationary (WSS) zero-mean real stochastic processes with known autocorrelation,

$$\begin{aligned} R_c(n) &= E\{c(m)c(n-m)\} \\ R_v(n) &= E\{v(m)v(n-m)\} \end{aligned} \tag{6}$$

where $E\{\cdot\}$ is the expected value operator. Under unknown target orientation and/or aspect angle, no specific impulse response can be discerned. However, we assume that the target impulse response $q(t)$ can be modeled as a WSS random process with known autocorrelation function,

$$R_q(n) = E\{q(m)q(n-m)\}. \tag{7}$$

In this case, the SCNR at the receive filter output can be expressed as [14]

$$\gamma = \frac{E\{|\mathbf{b}^T\mathbf{Q}\mathbf{z}|^2\}}{E\{|\mathbf{b}^T\mathbf{C}\mathbf{z}|^2\} + E\{|\mathbf{b}^T\mathbf{v}|^2\}} = \frac{\mathbf{b}^T\mathbf{R}_{q,z}\mathbf{b}}{\mathbf{b}^T\mathbf{R}_{c,z}\mathbf{b} + \mathbf{b}^T\mathbf{R}_v\mathbf{b}} \tag{8}$$

where

$$\begin{aligned} \mathbf{R}_{c,z} &= E\{\mathbf{C}\mathbf{z}\mathbf{z}^T\mathbf{C}^T\} \\ \mathbf{R}_v &= E\{\mathbf{v}\mathbf{v}^T\} \\ \mathbf{R}_{q,z} &= E\{\mathbf{Q}\mathbf{z}\mathbf{z}^T\mathbf{Q}^T\} \end{aligned} \tag{9}$$

which can be obtained by using the clutter, noise, and target autocorrelation, defined in (6) and (7). An iterative algorithm, proposed in [14], can be used to design the transmit waveform and the receive filter which maximize the SCNR in (8), and is reproduced below:

Given an initial value $\mathbf{z}_0$ of the transmit waveform $\mathbf{z}$, the transmit waveform and the receive filter can be optimized by repeating the following steps:

1. Compute $\mathbf{R}_{c,z} = E\{\mathbf{C}\mathbf{z}\mathbf{z}^T\mathbf{C}^T\}$ and $\mathbf{R}_{q,z} = E\{\mathbf{Q}\mathbf{z}\mathbf{z}^T\mathbf{Q}^T\}$.
2. Compute the Cholesky decomposition $\mathbf{R}_{c,z} + \mathbf{R}_v = \mathbf{L}_{c,z}\mathbf{L}_{c,z}^T$, where $\mathbf{L}_{c,z}$ is a lower triangular matrix.
3. Let $\mathbf{b} = (\mathbf{L}_{c,z}^{-1})^T\mathbf{p}(\mathbf{L}_{c,z}^{-1}\mathbf{R}_{q,z}(\mathbf{L}_{c,z}^{-1})^T)$ where $\mathbf{p}(\mathbf{A})$ denotes the principal component of matrix $\mathbf{A}$.
4. Compute $\mathbf{R}_{c,b} = E\{\mathbf{C}\mathbf{b}\mathbf{b}^T\mathbf{C}^T\}$ and $\mathbf{R}_{q,b} = E\{\mathbf{Q}\mathbf{b}\mathbf{b}^T\mathbf{Q}^T\}$.
5. Compute the Cholesky decomposition $\mathbf{R}_{c,b} + \mathbf{b}^T\mathbf{R}_v\mathbf{b}\cdot\mathbf{I} = \mathbf{L}_{c,z}\mathbf{L}_{c,z}^T$, where $\mathbf{I}$ is the identity matrix.
6. Let $\mathbf{z} = (\mathbf{L}_{c,z}^{-1})^T\mathbf{p}(\mathbf{L}_{c,z}^{-1}\mathbf{R}_{q,b}(\mathbf{L}_{c,z}^{-1})^T)$.
7. Normalize $\mathbf{z}$ to have the same energy as $\mathbf{z}_0$.

The iterations stop when the SCNR improvement becomes insignificant.

It is noted that for through-the-wall scenario, the free-space matrix formulation of (5) has to be modified to incorporate the wall's impulse response into the signal model [11, 12]. Wall transmission impulse response can be modeled as a complex gain which may vary over frequency [16]. Therefore, we represent the wall transmission impulse response, in general, as a linear time-invariant system. Then, the combined wall-target impulse response apparent to the radar is given by the convolution of the target impulse response with the two-way transmission impulse response of the wall[2]; the latter is assumed to be deterministic and known.[3] This combined response can be arranged in a convolution matrix $\tilde{\mathbf{Q}}$ having the same form as $\mathbf{Q}$ in (2). The optimization process can then proceed as in the case of free-space propagation, with $\mathbf{Q}$ replaced by $\tilde{\mathbf{Q}}$ in (8) and (9). It is noted that we consider only the wall transmission impulse response in the above model. The radar return from the wall itself arrives earlier than the return from the target. The wall reflections are assumed to have been either resolved from that of the target or mitigated using effective wall return removal techniques such as those recently proposed in [17], [18].

III. ELECTROMAGNETIC MODELING OF THE RIFLE

EM simulations were carried out using XFDTD®, a commercial full-wave EM simulator from Remcom Inc., for computing the impulse responses of an

[2]The linear relationship between the target and wall impulse responses holds, provided the target is sufficiently away from the wall so that interactions between the wall and the target are minimal.

[3]The wall parameters (thickness and dielectric constant) can be determined from the strong wall reflections [17], which can then be used to model the wall impulse response. Thus, the wall transmission impulse response is assumed known.

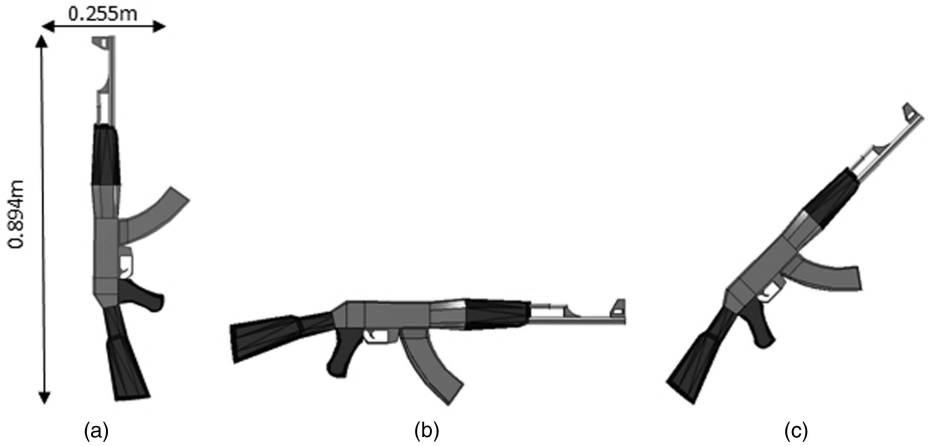

Fig. 1. AK-47 rifle at 0° azimuth. (a) Vertical. (b) Horizontal. (c) Inclined at 45°. Rifle dimensions also provided.

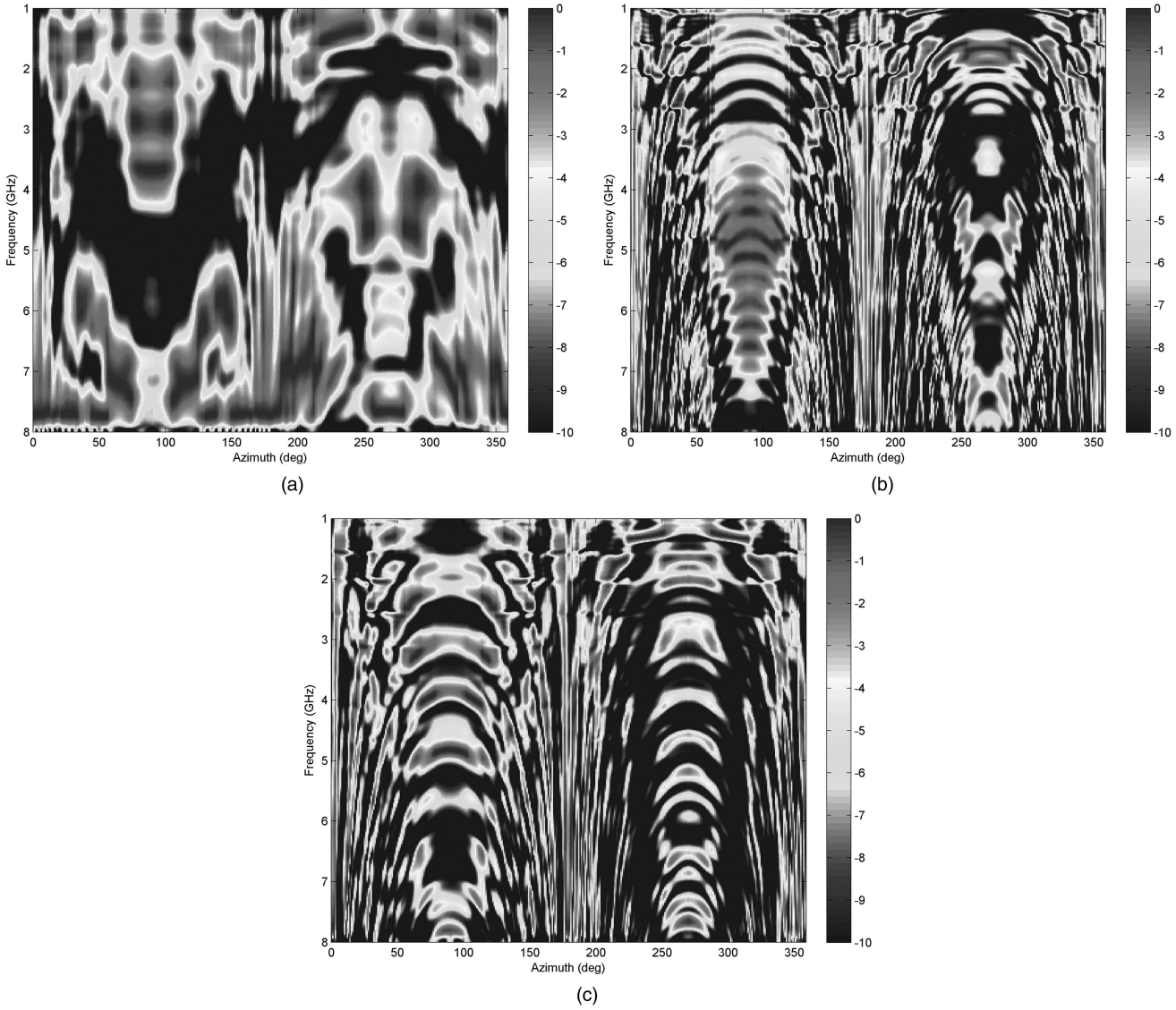

Fig. 2. Normalized frequency spectra of AK-47 rifle over 360° in azimuth. (a) Vertical. (b) Horizontal. (c) Tilted at 45°.

AK-47 assault rifle under plane wave excitation using vertical polarization corresponding to three orientations (vertical, horizontal, and inclined at 45°) for azimuthal aspect angles from 0° to 359° at 1° increment. It is noted that in case of nonhomogenous walls with metal rebars or grids, the

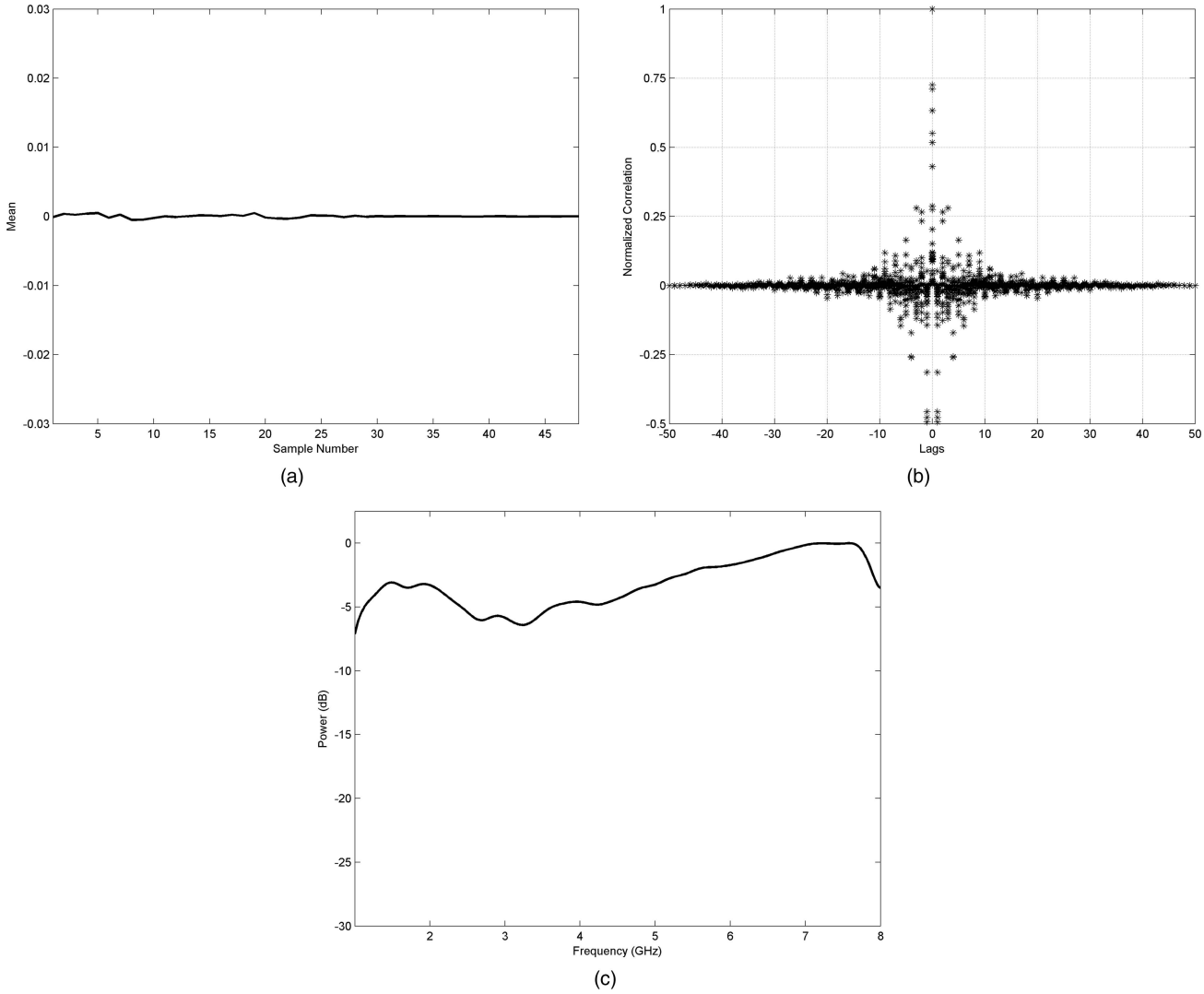

Fig. 3. (a) Mean, (b) values along various diagonals of correlation matrix, and (c) power spectrum of target random process.

use of dual-polarized or circularly polarized antennas may be preferred. The rifle model used consists of 3 mm cubical XFDTD mesh cells. In the model, the metallic parts of the rifle are assigned perfect electric conductors and the wooden components are chosen to be lossless with an assigned permittivity of 2. The rifle dimensions and the simulation geometry for the three different orientations are provided in Fig. 1 for 0° aspect. The azimuthal aspect angle is measured in a counterclockwise fashion. The incident waveform was chosen to be a vertically polarized modulated Gaussian with frequency content ≥ 10 dB over the 0.5 GHz to 10 GHz frequency range. The copolarized scattered field was collected over 360° in azimuth under monostatic operation for each orientation. The corresponding target impulse responses were obtained by deconvolving the transmitted waveform from the scattered fields. More specifically, for each target orientation and azimuth angle, the corresponding target impulse response $\mathbf{q}$ was obtained as the least squares solution [11],

$$\mathbf{q} = (\mathbf{Z}^T\mathbf{Z})^{-1}\mathbf{Z}^T\mathbf{s} \tag{10}$$

where $\mathbf{Z}$ is a convolution matrix, identical in structure to (2), containing the incident modulated Gaussian waveform, and $\mathbf{s}$ is the target return vector. In order to avoid any numerical modeling errors at both the lower and higher ends of the frequency range, both the incident waveform and the target returns were bandpass filtered with a passband from 1.2 to 7.8 GHz prior to deconvolution. All of the impulse responses were resampled so that there is only one sample per range bin. The sampling period of the resultant impulse responses is 0.0625 ns.

The normalized magnitude spectra of the AK-47 rifle for the three orientations corresponding to the aspect angles between 0° and 359° are depicted in Fig. 2. It is clear from Fig. 2 that the target response varies considerably as a function of orientation and aspect angle. Assuming the target impulse responses corresponding to the various orientations and aspect

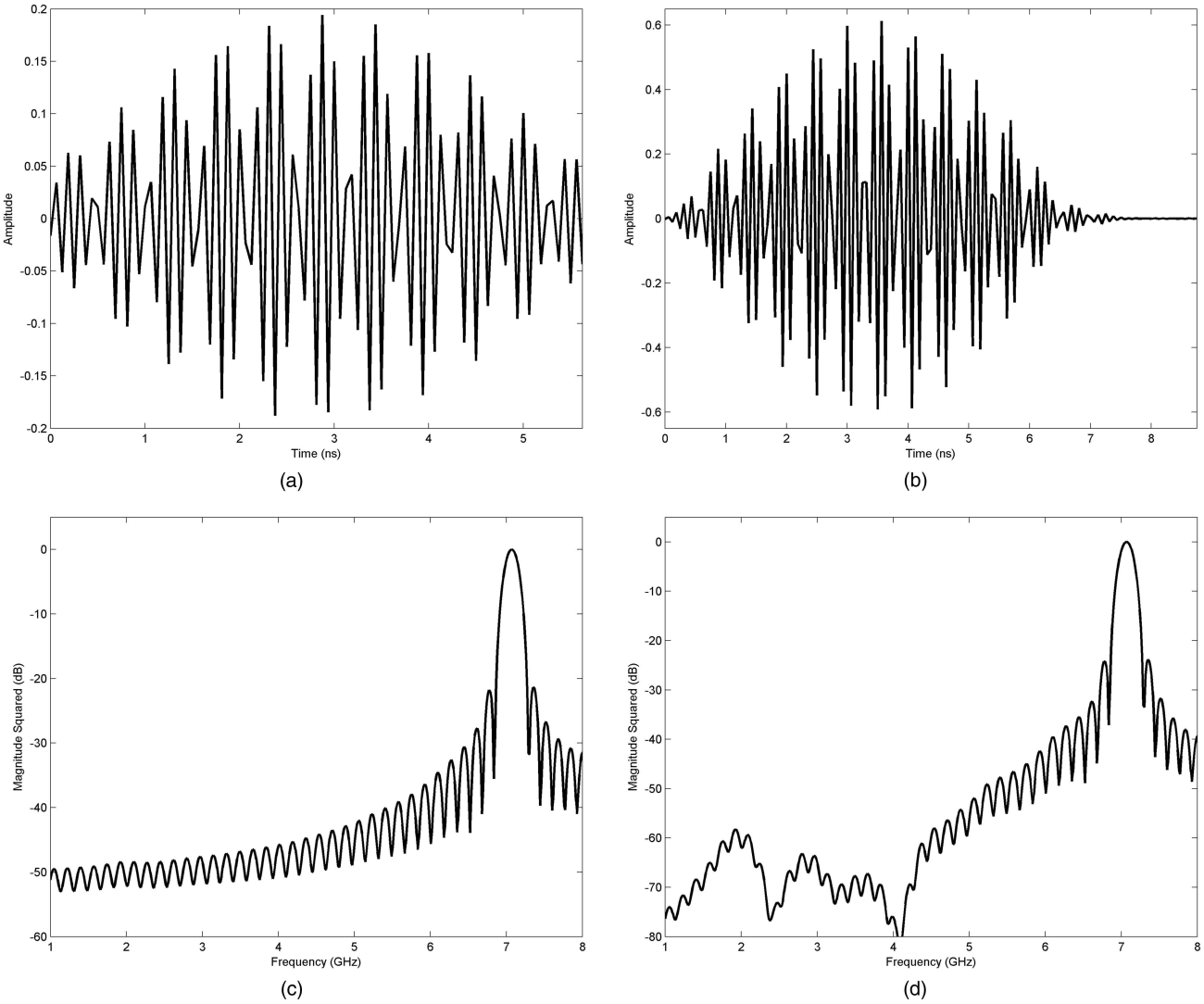

Fig. 4. Free-space propagation. (a) Designed waveform. (b) Impulse response of receive filter. (c) Magnitude of designed waveform spectrum. (d) Magnitude of designed receive filter spectrum.

angles to be sample functions of a random process, we compute the mean and correlation matrix of the random process. The mean is depicted in Fig. 3(a), whereas Fig. 3(b) shows the values along each diagonal of the correlation matrix. It is noted that the main diagonal is indexed by a lag of zero, while the positive and negative lags indicate diagonals above and below the main diagonal, respectively. We observe that the mean is roughly independent of time. On the other hand, the variation in values along each diagonal of the correlation matrix is negligible, except in a small neighborhood around zero lag. Thus, applying the waveform design technique of Section II to the AK-47 rifle target process involves an approximation; that is, ignoring the dependence of the correlation of the target random process on the sampling instants and treating it as WSS. The power spectrum of the target process is shown in Fig. 3(c).

IV. DESIGN EXAMPLES

In this section we present waveform design examples based on the stochastic target model for white-noise only and clutter-plus-noise cases under both free-space and through-the-wall propagation scenarios. In order to evaluate the detection performance of the designed waveform-filter combination as a function of target orientation and aspect angle, we choose the performance measure to be the target orientation and aspect dependent SCNR at the output of the receive filter, which using (5) can be expressed as

$$\text{SCNR} = \frac{|\mathbf{b}^T\mathbf{Q}\mathbf{z}|^2}{E\{|\mathbf{b}^T\mathbf{C}\mathbf{z}|^2\} + E\{|\mathbf{b}^T\mathbf{v}|^2\}} = \frac{\mathbf{b}^T\mathbf{Q}\mathbf{z}\mathbf{z}^T\mathbf{Q}^T\mathbf{b}}{\mathbf{b}^T\mathbf{R}_{c,z}\mathbf{b} + \mathbf{b}^T\mathbf{R}_v\mathbf{b}}. \tag{11}$$

The performance of the designed waveform is compared with that of a chirp waveform spanning the 1–8 GHz band of interest and having the same

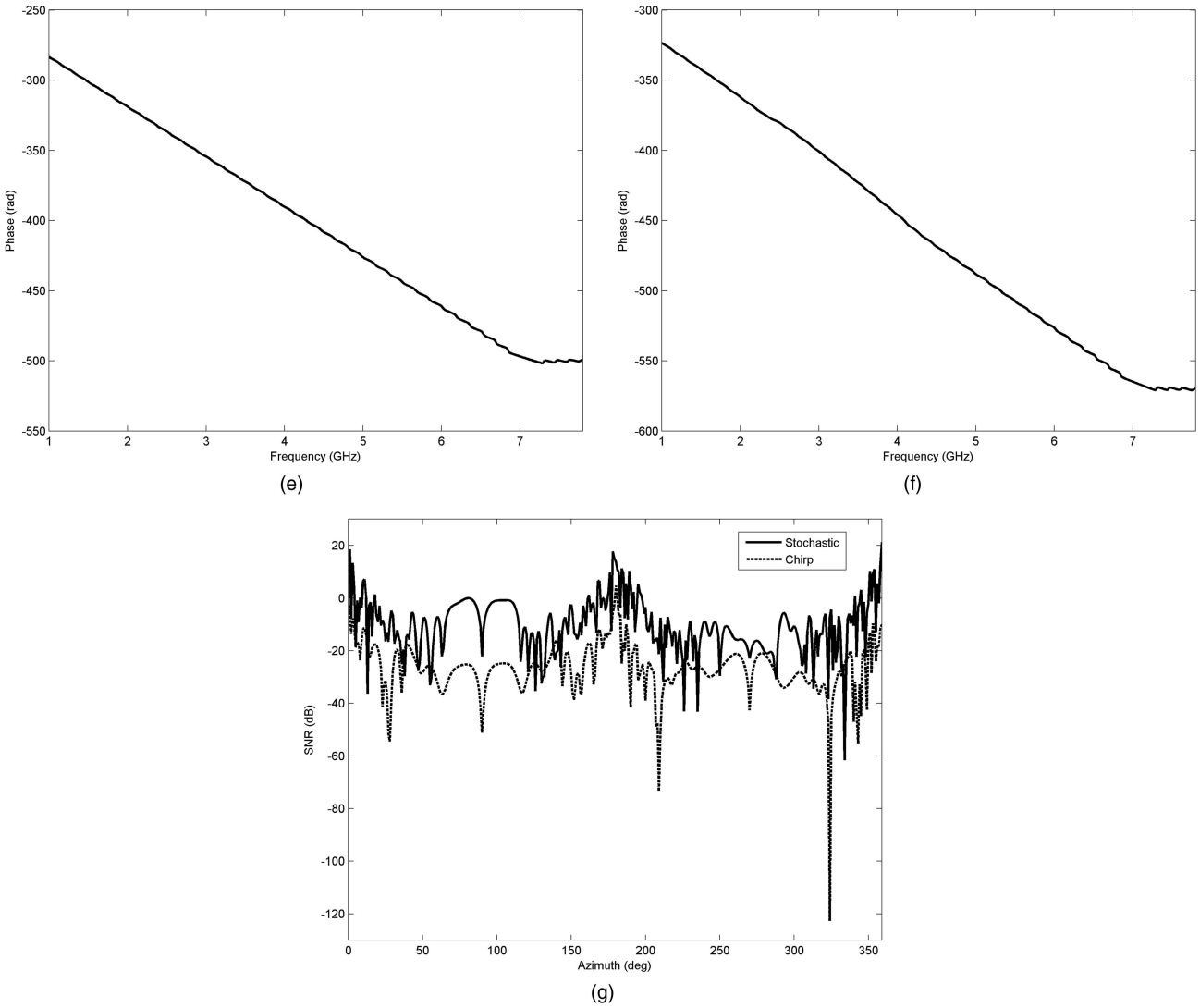

Fig. 4 *(continued)*. (e) Phase of designed waveform spectrum. (f) Phase of designed receive filter spectrum. (g) SNR improvement over chirp as function of azimuth angle for rifle tilted at 45° using stochastic approach.

duration and energy. Also, identical noise variance was used in all cases.

A. Clutter-Free Case

The stochastic model based waveform-filter combination was first designed for the detection of the AK-47 rifle in the presence of white noise only under free-space propagation. The waveform vector is chosen to be of length $N_z = 91$ and the target impulse response has a length $N_q = 51$. Thus, the length N_s of the receive filter was specified as 141. The algorithm converged in 8 iterations. The designed transmit waveform and receive filter are shown in Figs. 4(a) and (b), respectively. The magnitude and phase of the designed waveform and the receive filter spectra are depicted in Figs. 4(c)–(f). We observe that the waveform has focused all of its energy in a narrow band of frequencies which coincides with a high response region of the target power spectrum shown in Fig. 3(c). For illustration, the signal-to-noise ratio (SNR) as a function of azimuth aspect angle for the rifle inclined at 45° using the designed and chirp waveforms is provided in Fig. 4(g). It is noted that the receive filter in the case of the chirp for this and all subsequent examples is matched to the transmitted chirp waveform (ideal for detection of point targets). From Fig. 4(g), we observe that the waveform-filter design based on the stochastic target model significantly outperforms the chirp for most of

TABLE I
Average SNR Improvement over a Chirp Waveform for Noise-Only Case

Target Orientation	Average SNR Improvement (dB)	
	Free-Space Operation	Through-the-Wall Operation
Vertical	23.92	48.60
Horizontal	21.79	44.59
45°	16.27	39.02

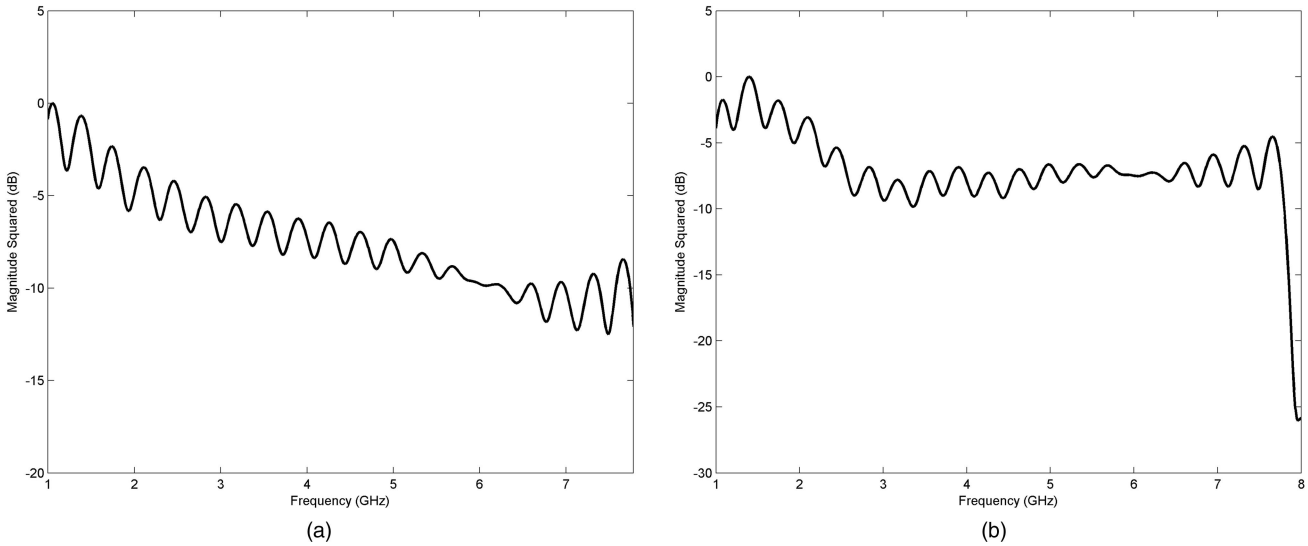

Fig. 5. (a) Two-way brick wall transmission frequency response. (b) Power spectrum of through-the-wall target process.

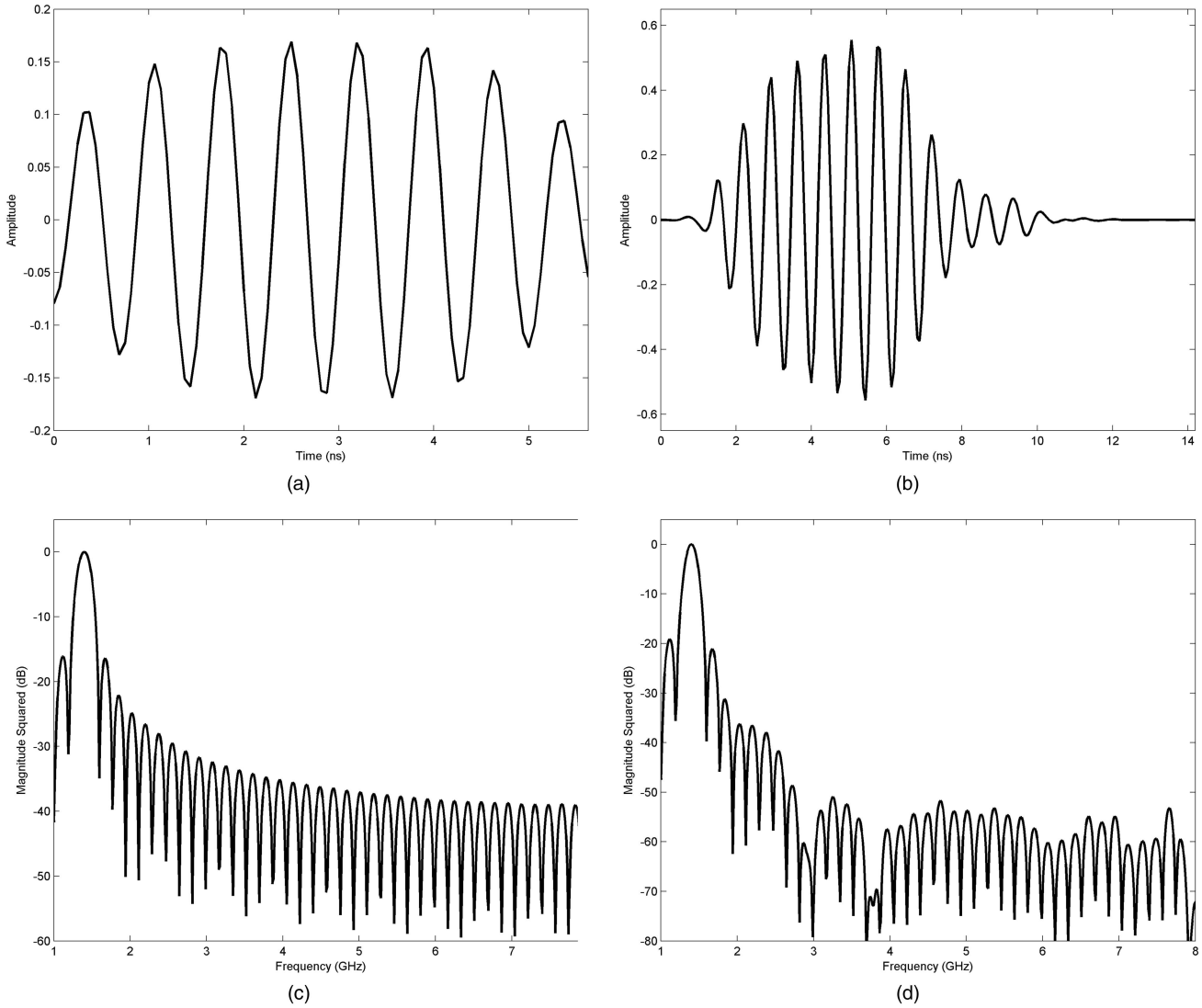

Fig. 6. Through-the-wall propagation. (a) Designed waveform. (b) Impulse response of receive filter. (c) Magnitude of designed waveform spectrum. (d) Magnitude of designed receive filter spectrum.

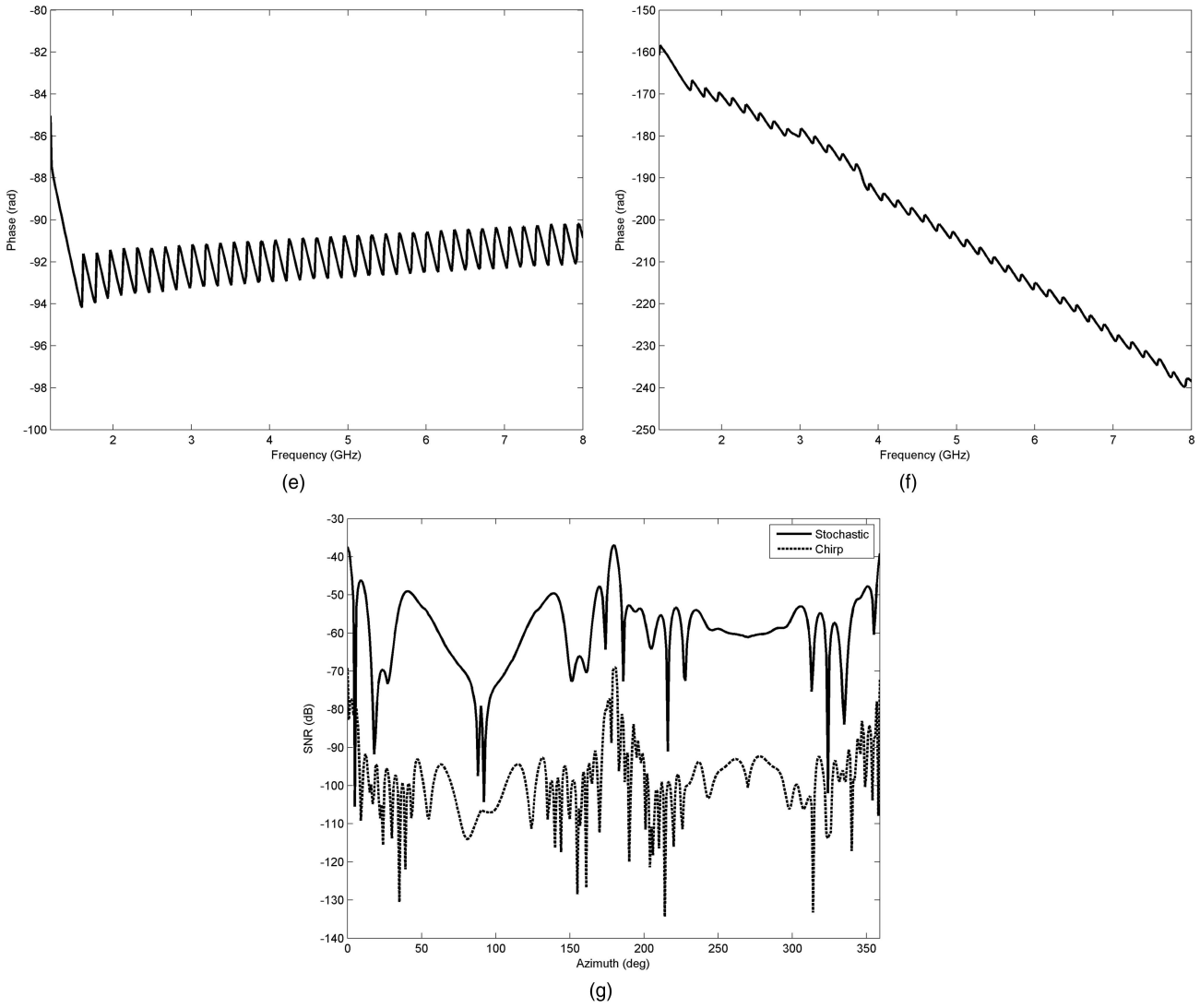

Fig. 6 *(continued).* (e) Phase of designed waveform spectrum. (f) Phase of designed receive filter spectrum. (g) SNR improvement over chirp as function of azimuth angle for rifle tilted at 45° behind brick wall using stochastic approach.

the angles. On average, the stochastic-based design provides an improvement of 16.27 dB over the chirp waveform. The designed waveform provides improved performance for the vertical and horizontal rifles as well, as indicated in Table I, which lists the average SNR improvement of the designed waveform-filter combination over the chirp with conventional matched filter for each considered target orientation.

Next, the AK-47 rifle was placed behind a homogeneous brick wall of 0.194 m thickness. The transmission impulse response of the wall was also computed using XFDTD®, with relative permittivity and loss tangent of brick assigned as 4.79 and 0.036, respectively. Fig. 5 shows the magnitude of the two-way wall transmission frequency response and the power spectrum of the through-the-wall target process. The stochastic model based detection waveform and receive filter were designed for the through-the-wall scenario in case of noise only, and are shown in Fig. 6(a) and (b), respectively. The optimization algorithm converged in 8 iterations. The waveform vector was chosen to be of length $N_z = 91$ and the combined wall-target impulse response has a length $N_q = 138$. Thus, the length N_s of the receive filter for through-the-wall scenario was specified as 228. The magnitude and phase of the designed waveform and the receive filter spectra are depicted in Figs. 6(c)–(f). Comparing Figs. 6(c) and 4(c), we observe that the designed through-the-wall waveform focuses its energy in a narrow frequency band towards the lower end of the 1–8 GHz band. This is also evident by comparing the time-domain waveforms in Figs. 6(a) and 4(a). This is not surprising since, as seen from Fig. 5, the wall attenuates the higher frequencies more than the lower frequencies, resulting in higher combined wall-target responses at lower frequencies over various aspect angles and orientations. The SNR at the output of the receive filter due to the stochastic model based through-the-wall waveform and a chirp of same energy and duration is shown

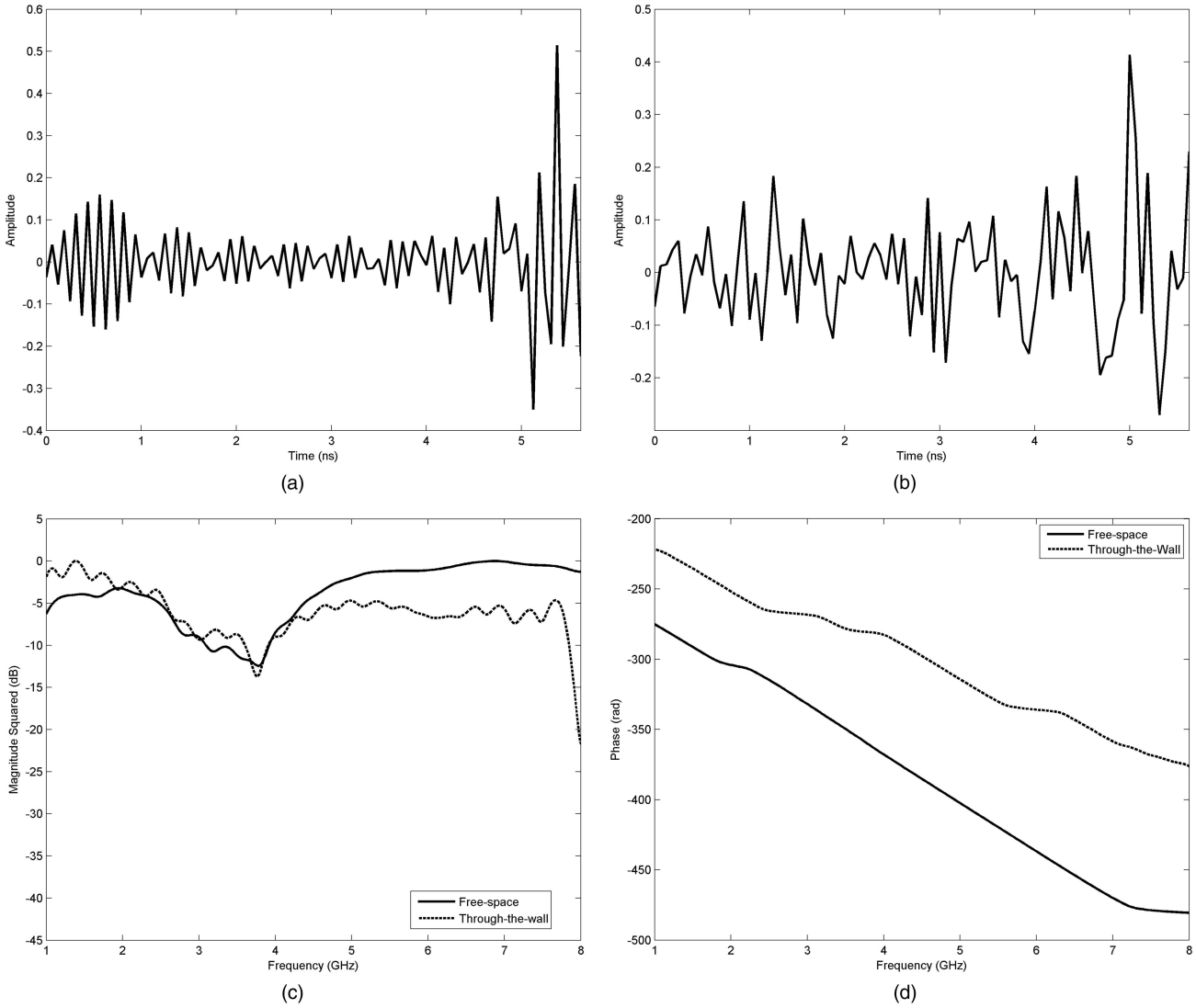

Fig. 7. SCNR = +10 dB. (a) Designed free-space waveform. (b) Designed through-the-wall waveform. (c) Magnitude of designed free-space and through-the-wall waveform spectra. (d) Phase of designed free-space and through-the-wall waveform spectra.

in Fig. 6(g). We note that although the overall SNR has degraded due to the presence of the wall, the improvement over a chirp is significantly higher than that of the free-space case. This is attributed to the facts that 1) the target response at higher frequencies undergoes a larger attenuation on propagation through the wall and the energy invested by the chirp at the higher frequencies in the 1–8 GHz band does not payoff, and 2) the conventional matched filter for the chirp presents more of a mismatch in the case of the through-the-wall target response, which is more extended compared with the free-space response due to the convolution with the wall transmission response. Average SNR improvement of the stochastic model based waveform over the chirp for the three rifle orientations under through-the-wall propagation is provided in Table I, which shows substantial improvement over the chirp for each orientation.

B. Clutter-Plus-Noise Case

In the absence of any proper statistical characterization of clutter for through-the-wall scenarios and the lack of supporting arguments to use other distributions, the clutter is assumed to be zero-mean white Gaussian process [10, 11]. The clutter and the noise are assumed to be of independent samples. The clutter-to-noise-ratio (CNR) was varied from −20 dB to +40 dB in 10 dB increments, and the stochastic model based waveform for the rifle was designed for each value of the CNR, both in the absence and presence of the brick wall. The optimization algorithm converged in 10 iterations at the most.

Table II provides the average SCNR improvement over the chirp waveform as a function of CNR for the three rifle orientations under free-space propagation, while that for through-the-wall propagation is provided in Table III. From Tables II

TABLE II
Average SCNR Improvement over a Chirp Waveform as a Function of CNR for Free-Space Propagation

Average SCNR Improvement (dB)							
Target Orientation	CNR (dB)						
	−20	−10	0	+10	+20	+30	+40
Vertical	23.91	14.36	10.71	10.08	10.3	10.30	10.28
Horizontal	22.02	7.14	3.42	3.06	3.01	2.85	3.06
45°	16.41	8.72	6.68	6.14	6.18	6.22	6.22

TABLE III
Average SCNR Improvement over a Chirp Waveform as a Function of CNR for Through-the-Wall Propagation

Average SCNR Improvement (dB)							
Target Orientation	CNR (dB)						
	−20	−10	0	+10	+20	+30	+40
Vertical	47.45	44.15	37.84	33.98	33.26	33.24	33.24
Horizontal	43.22	33.95	27.64	24.02	23.58	23.52	23.49
45°	38.09	34.91	24.45	21.29	20.78	20.75	20.76

and III, we observe that when the clutter is weaker than the noise, the optimized waveform-filter combination provides comparable performance to the corresponding noise-only design under both free-space and through-the-wall propagation. For the case of comparable noise and clutter, the designed transmission waveforms and filters (not shown) reveal a broadening of the frequency peaks and/or appearance of additional peaks compared with their noise-only counterparts. When the clutter becomes significant, i.e., for a CNR of +10 dB and beyond, the corresponding designed waveform-filter combinations yield similar SCNR improvement over a chirp. This is in compliance with the degenerate case of negligible noise and significant clutter, described in [19], wherein all transmission waveforms yield identical value for the SCNR of (11), provided an appropriate receiver matched filter is used. In both Tables II and III, a value other than 0 dB is obtained at the SCNR improvement saturation point due to the use of the conventional matched filter for the chirp waveform. Moreover, the difference in saturation point values between free-space and through-the-wall propagation is attributed to the longer extent of the combined wall-target response, which presents a greater mismatch for the conventional point-target based matched filter for the chirp. The stochastic model based detection waveforms for the free-space and through-the-wall scenarios corresponding to a CNR of +10 dB are shown in Fig. 7(a) and (b), respectively. We observe that the waveforms are wideband in nature. The corresponding magnitude and phase responses are plotted in Figs. 7(c) and (d). From Fig. 7(c), it is clear that the waveform energy distribution matches the respective power spectra of the free-space and through-the-wall target processes.

V. CONCLUSION

In this correspondence, we presented waveform design based on target signature exploitation for detection of weapons under unknown target orientation and azimuthal aspect angle. Performance of the designed waveform was compared with that of the widely used chirp waveform of equal energy and duration. Both cases of noise-only and clutter-plus-noise in free-space and through-the-wall propagation were considered. Using an AK-47 weapon as a target, we showed that the stochastic-based waveform significantly outperforms the chirp in terms of the SCNR at the output of the receive filter, which implies an enhanced detection performance.

ACKNOWLEDGMENT

The authors would like to thank Dr. Traian Dogaru, U.S. Army Research Lab, for providing us with the AK-47 rifle mesh grid, and Dr. Wenji Zhang, Villanova University, for performing the XFDTD® simulations for computing the target impulse responses.

FAUZIA AHMAD
MOENESS G. AMIN
Radar Imaging Lab
Center for Advanced Communications
Villanova University
800 Lancaster Ave.
Villanova, PA 19085
E-mail: (fauzia.ahmad@villanova.edu)

REFERENCES

[1] Currie, N. C., et al.
Infrared and millimeter-wave sensors for military special operations and law enforcement applications.
International Journal of Infrared and Millimeter Waves, **17**, 7 (1996), 1117–1138.

[2] Agurto, A., et al.
A review of concealed weapon detection and research in perspective.
In *Proceedings of the 2007 IEEE International Conference on Networking, Sensing, and Control*, London, Apr. 2007, 443–448.

[3] Kruger, M.
Transparent urban structures enabling capability program.
Office of Naval Research, 2007. [Online], available: http://www.onr.navy.mil/~/media/Files/Funding-Announcements/BAA/07-035.ashx.

[4] Amin, M. (Ed.)
Through-the-Wall Radar Imaging.
Boca Raton, FL: CRC Press, 2010.

[5] Amin, M. and Sarabandi, K. (Eds.)
IEEE Transactions on Geoscience and Remote Sensing (special issue on remote sensing of the building interior).
47, 5 (May 2009), 1270–1420.

[6] Sheen, D. M., McMakin, D. L., and Hall, T. E.
Three-dimensional millimeter-wave imaging for concealed weapon detection.
IEEE Transactions on Microwave Theory Techniques, **49**, 9 (2001), 1581–1592.

[7] Catapano, I. and Crocco, L.
An imaging method for concealed targets.
IEEE Transactions on Geoscience and Remote Sensing, **47**, 5 (May 2009), 1301–1309.

[8] Dogaru, T. and Le, C.
Through-the-wall small weapon detection based on polarimetric radar techniques.
U.S. Army Research Lab, Technical Report ARL-TR-5041, Dec. 2009. Available: http://www.dtic.mil/cgibin/GetTRDoc?Location=U2&doc=GetTRDoc.pdf&AD=ADA510201.

[9] Gjessing, D. T.
Target Adaptive Matched Illumination RADAR: Principles and Applications (IEE Electromagnetic Waves Series 22).
London: Peregrinus Ltd., 1986.

[10] Garren, D. A.
Enhanced target detection and identification via optimized radar transmission pulse shape.
IEE Proceedings—Radar, Sonar and Navigation, **148**, 3 (June 2001), 130–138.

[11] Estephan, H., Amin, M. G., and Yemelyanov, K. M.
Optimal waveform design for improved detection and classification of targets for through-the-wall radar applications.
IEEE Transactions on Geoscience and Remote Sensing, **48**, 7 (2010), 2930–2941.

[12] Ahmad, F. and Amin, M. G.
Matched-illumination waveform design for a multistatic through-the-wall radar system.
IEEE Journal of Selected Topics in Signal Processing, **4**, 1 (2010), 177–186.

[13] Romero, R. A., Bae, J. H., and Goodman, N. A.
Theory and application of SNR- and MI-based matched illumination waveforms.
IEEE Transactions on Aerospace and Electronic Systems, **47**, 2 (2011), 912–927.

[14] Chen, C-Y. and Vaidyanathan, P. P.
MIMO radar waveform optimization with prior information of the extended target and clutter.
IEEE Transactions on Signal Processing, **57**, 9 (Sept. 2009), 3533–3544.

[15] Ahmad, F. and Amin, M. G.
Maximin robust radar waveform design for detection of weapons.
In *Proceedings of the 18th European Signal Processing Conference*, Aalborg, Denmark, Aug. 2010.

[16] Muqaibel, A. and Safaai-Jazi, A.
Characterization of wall dispersive and attenuative effects on UWB radar signals.
Journal of the Franklin Institute, **345** (Sept. 2008), 640–658.

[17] Hoorfar, A. and Thajudeen, C.
Multilayer wall parameter estimation and mitigation techniques in through-wall imaging radar.
In *Proceedings of the IEEE Antennas and Propagation Society International Symposium and URSI Radio Science Meeting*, Toronto, Canada, July 2010.

[18] Dehmollaian, M. and Sarabandi, K.
Refocusing through building walls using synthetic aperture radar.
IEEE Transactions on Geoscience and Remote Sensing, **46**, 6 (June 2008), 1589–1599.

[19] Pillai, S. U., et al.
Optimal transmit receiver design in the presence of signal-dependent interference and channel noise.
IEEE Transactions on Information Theory, **46**, 2 (Mar. 2000), 577–584.

Emitter Localization Given Time Delay and Frequency Shift Measurements

Given time and frequency differences of arrival measurements, we estimate the position and velocity of an emitter by jointly eliminating nonlinear nuisance parameters with an orthogonal projection matrix. Although simulation results show that this estimator does not always perform as well as the two-step estimator, the benefit is its computational simplicity. Whereas the complexity of the two-step estimator increases cubically with respect to the number of sensors, the complexity of the proposed estimator increases quadratically.

I. INTRODUCTION

Estimating the location of an emitter with a passive sensor array has been of considerable interest for many years, and has found many applications in several fields including radar, sonar, wireless communications, satellites, airborne systems, and acoustics [1–11]. With the common indirect estimation approach [1, 2], one or more parameters (e.g., angle or time of arrival) are measured, and the emitter parameters (position and/or velocity) are then determined. A different approach is to estimate the emitter parameters directly from the observations [10, 11]. Herein, we focus on the former approach assuming a stationary passive sensor array and a moving emitter.

Given the measurements of time differences of arrival (TDOAs) and frequency differences of arrival (FDOAs) between pairs of observed signals, the goal is to estimate the source position and velocity.[1] Weinstein proposed an estimation technique which is applicable for a linear array only and assumes a source in the far-field region [5]. The estimation procedure suggested by Ho and Xu [9] extended the two-step approach of Chan and Ho [8] by taking

[1]The TDOAs and FDOAs are obtained by maximizing the ambiguity function [12]. Their statistical properties are discussed in [13], [14], and [16], assuming a known, an unknown deterministic, and a random transmitted signal, respectively.

Manuscript received April 1, 2010; revised November 1, 2010 and May 3, 2011; released for publication June 24, 2011.

IEEE Log No. T-AES/48/2/943861.

Refereeing of this contribution was handled by W. Koch.

The work of A. Amar and G. Leus was supported in part by NWO-STW under the VICI program (Project 10382). The work of B. Friedlander was supported by the National Science Foundation under Grant CCF-0725366.